X-ray structural characterization, Raman and thermal analysis of $LiNaSO_4$. The phase diagram of the Li_2SO_4-Na_2SO_4 system

2002 J. Phys.: Condens. Matter 14 5211

(http://iopscience.iop.org/0953-8984/14/20/316)

INSTITUTE OF PHYSICS PUBLISHING JOURNAL OF PHYSICS: CONDENSED MATTER

J. Phys.: Condens. Matter **14** (2002) 5211–5220 PII: S0953-8984(02)33222-3

X-ray structural characterization, Raman and thermal analysis of $LiNaSO_4$. The phase diagram of the Li_2SO_4–Na_2SO_4 system

Jorge Mata, Xavier Solans, M Teresa Calvet, Judit Molera and Mercè Font-Bardia

Departament de Cristallografia, Universitat de Barcelona, E-08028 Barcelona, Spain

Received 30 January 2002
Published 9 May 2002
Online at stacks.iop.org/JPhysCM/14/5211

Abstract

An accurate structural study on the β-phase of $LiNaSO_4$ was carried out. This study shows that twin crystals are usually obtained when crystallization takes place from solution, which explains the observed low spontaneous polarization. Raman scattering of Li_2SO_4, Na_2SO_4 and $LiNaSO_4$ is explained from the structural data. The phase diagram of the binary system Li_2SO_4–Na_2SO_4 was determined by x-ray diffraction and the DTA method. Mixed crystals of the low-temperature phase of $Li_{2-x}Na_xSO_4$ with $1 \leqslant x \leqslant 1.22$ were observed for the first time. The temperatures of the process in this diagram are high, depending on the cooling rate. A more congruent diagram was obtained working at a lower cooling rate.

1. Introduction

The system Li_2SO_4–Na_2SO_4 has been widely studied because of the fast-ionic conductivity of the observed phases at high temperature. The first phase diagram of this system was determined by Nacken [1] and later revised in [2, 3]. An intermediate compound is observed in this phase diagram, $LiNaSO_4$. In [1] and [2] the decomposition of the α-$LiNaSO_4$ to give α-Li_2SO_4 + α-Na_2SO_4 during a cooling process it is considered, while in [3] a phase transition between the α- and β-phase is considered.

Li_2SO_4 undergoes a phase transition at 851 K [4]. The structure of high-temperature phase (α-phase) was determined at 908 [5], 883 [6] and 873 K [7], while the low-temperature phase (β-phase) was determined at room temperature [8]. From thermal [4] and electrical conductivity [9] and from ion diffusion [4, 10] studies of Li_2SO_4 it is concluded that the α-phase is a fast-ionic conductor. From the previously mentioned structural studies it is concluded that the conduction mechanism is a mixture of the paddle wheel model and the percolation model.

Na_2SO_4 undergoes four phase transitions in the range 700–293 K. The phases in order of decreasing temperature are named I, II, III, IV and V. The transition temperatures are 506, 498, 493 and 483 K in a cooling process according to the results from thermal analyses and electrical

conductivity [11–15]. Phase IV (range 493–483 K) is not observed by x-ray diffraction. The structure of phase I was determined at 693 [16] and 543 K [17, 18], phases II and III at 493 and 463 K [17], respectively, and phase V at 293 K [17, 19]. The discrepancies between the phase temperature transition and the temperature of crystal structure determination are due to the fact that the transition temperature depends on the cooling rate.

The structure of α-$LiNaSO_4$ was determined at 823 K [4]. Ion diffusion [10] and conductivity studies [20] show that this phase is also a fast-ionic conductor. The structure of the β-phase was determined by Morosin and Smith [21], but NMR results [22] seem to contradict this structure. Raman scattering of $LiNaSO_4$ has been widely studied [23–25]. Recently, the pressure-induced phase transition has also been studied [26].

Attempts to prepare $LiNaSO_4$ from melt and from solution gave results which did not agree with the phase diagram, so we decide to review the phase diagram and the structure of β-phase of $LiNaSO_4$.

2. Experimental details

2.1. Synthesis

The lithium sulfate and sodium sulfate were Aldrich and Fluka products, respectively (purity = 99.99%). The lithium sodium sulfate was obtained via the reaction of Na_2SO_4 with Li_2SO_4 in aqueous solution and via the melting of Na_2SO_4 and Li_2SO_4 at 913 K and posterior quenching or cooling process (1 day). The molar ratio between the sodium and lithium sulfates was 1:1. The obtained compound was analysed by ICP (induced condensed plasma) with a Jobin–Yvon analyser. Crystals were obtained by slow evaporation at 313 K.

2.2. Raman scattering

Raman spectra were excited on the powder sample using a Jobin–Yvon T64000 spectrometer, and an argon-ion laser excitation. The detector used was a Control Data CDC. The spectra were recorded with the 514.5 nm line and a light power equal to 1.05 W. All spectra were calibrated against selected neon lines. The position, half-width and relative intensity of each peak was determined, assuming it to be a Lorentzian function (the Gaussian contribution is negligible).

2.3. X-ray structure determination

Diffraction data were collected on a MAR345 automated diffractometer equipped with a graphite monochromator and image plate detector. The ϕ scan technique was used to record the intensities. Details of the structure determination are listed in table 1. The unit-cell parameters were obtained by a least-squares fit to the automatically centred settings from 1173 reflections ($3^\circ < \theta < 33^\circ$).

The structures were solved by direct methods using the SHELXS-97 computer program [27], and refined by the full-matrix least-squares method using the SHELXL-93 computer program [28]. The function minimized was $w||\mathrm{Fo}|^2 - |\mathrm{Fc}|^2|^2$, where the weighting scheme was $w = [\sigma^2(I) + (0.032P)^2 + 0.0928P]^{-1}$ and $P = (|\mathrm{Fo}|^2 + 2|\mathrm{Fc}|^2)/3$. Final refinement gave an $R1$ factor equal to 0.018, but the Flack coefficient [29] was 0.38(8), which indicated a chiral twin in the sample. Attempts using the enantiomorph coordinates or different twin laws failed, except when the twin law (1,0, 0/0, 1, 0/0, 0, −1) was used, which led to a final Flack coefficient equal to zero and a relative batch scale factor equal to 0.586 for the atomic coordinates listed in table 2 and 0.414 for the twinned coordinates.

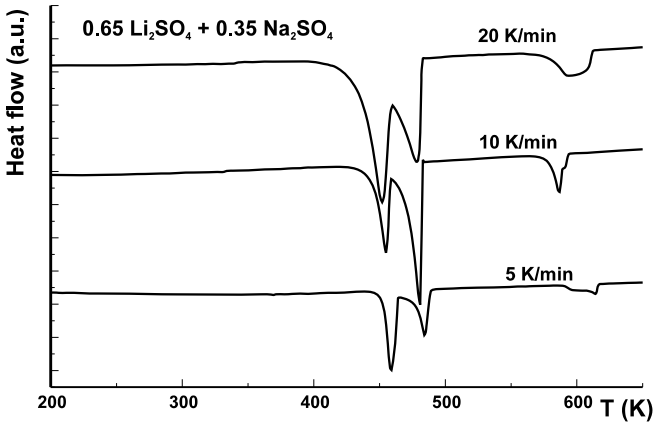

Figure 1. DTA results obtained at different cooling rates.

Table 1. Crystal data and structure refinement for $LiNaSO_4$.

Empirical formula	$LiNaSO_4$
Formula weight	125.99
Temperature (K)	293(2)
Wavelength (Å)	0.710 69
Crystal system, space group	Trigonal, $P31c$
a (Å)	7.6190(10)
c (Å)	9.8490(10)
Volume (Å^3)	495.13(10)
Z, ρ_c (mg m^{-3})	6, 2.535
μ (mm^{-1})	0.946
$F(000)$	372
Crystal size (mm^3)	$0.3 \times 0.2 \times 0.2$
Θ range for data collection (°)	3.09–33.13
Index ranges	$0 \leqslant h \leqslant 11$, $-9 \leqslant k \leqslant 0$, $-14 \leqslant l \leqslant 15$
Reflections collected/unique (R(int) = 0.0139)	1173/728
Data/parameters	701/66
Goodness of fit on F^2	1.161
R indices (all data)	$R1 = 0.018$, $wR2 = 0.053$
Absolute structure parameter	0.0(5)
Extinction coefficient	0.017(9)
Largest diff. peak and hole (e Å^{-3})	0.385 and −0.336

2.4. Phase diagram

The phase diagram of the Li_2SO_4–Na_2SO_4 system was based on the results of phase analysis and differential thermal analysis (DTA) and thermogravimetry (TG) measurements. The thermal analysis for the temperature range 298–1175 K was carried out in a Netzsch 409 DTA and TG. The sample was a mixture of $Li_2SO_4 \cdot H_2O$ and Na_2SO_4. The measured water loss by TG was used as an analysis of the composition of the mixture. Different warming and cooling rates were used (figure 1). The best-defined peaks were obtained at 10 K min^{-1} during the cooling process, so the phase diagram was elaborated at this rate. The weights of samples were about 80 mg and the reference material was alumina. The phase analyses were made with a Siemens D500 at different temperatures, using Cu Kα radiation and a secondary monochromator.

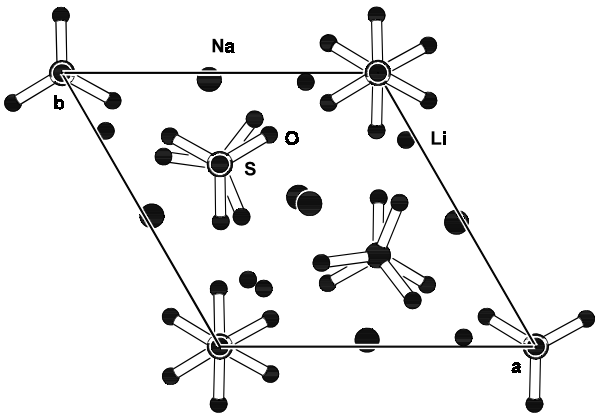

Figure 2. Projection of the unit-cell content of β-$LiNaSO_4$ down the c-axis.

Table 2. Atomic coordinates ($\times 10^4$) and equivalent isotropic displacement parameters ($Å^2 \times 10^3$) for $LiNaSO_4$. $U(eq)$ is defined as one-third of the trace of the orthogonalized U_{ij} tensor.

	x	y	z	$U(eq)$
Na	9 766(1)	4 543(1)	4 881(1)	20(1)
S(1)	10 000	10 000	17(1)	8(1)
S(2)	6 667	3 333	1 967(1)	8(1)
S(3)	3 333	6 667	2 629(1)	8(1)
O(1)	10 000	10 000	1 544(2)	10(1)
O(2)	6 667	3 333	3 451(2)	17(1)
O(3)	3 333	6 667	1 143(2)	18(1)
O(4)	7 898(2)	8 909(2)	−478(1)	14(1)
O(5)	7 742(2)	5 427(2)	1 450(1)	19(1)
O(6)	5 256(2)	8 313(3)	3 145(2)	28(1)
Li	9 670(5)	7 552(5)	2 605(3)	18(1)

The experiment was a warming process from 298 to 1175 K. The samples were left for 10 min at the melt point, followed by a cooling process with a cooling rate of 10 K min^{-1} between the same temperatures. The patterns were measured at different temperatures and the samples were left for 10 min at measuring temperature in order to stabilize the equipment and the sample. The step size was 0.025°, the time of each step 10 s and the 2θ range 10°–60°. Cell parameters from powder diffraction were refined with the FULLPROF computer program [30] using as structural model the structures obtained by single-crystal diffraction.

3. Results and discussion

Figures 2 and 3 show two projections of the cell content. The present atomic coordinates can be obtained from those of Morosin and Smith [21] by rotation about a twofold axis parallel to the $\boldsymbol{c}$-axis ($x = 1 - x_M$; $y = 1 - y_M$; $z = z_M$). From this is deduced that the two structures have the same chirality, but this twofold axis is not a crystallographic symmetry. Two hypotheses can be derived from this result: (I) the two phases are different or (II) the chirality of the structure of Morosin was not solved and was erroneous. (The $R1$ agreement coefficient of Morosin is higher and the thermal factors for S(1) and O(2) are nonpositive definite.) From the second hypothesis and as the product of the twofold axis parallel to $\boldsymbol{c}$ and the inversion

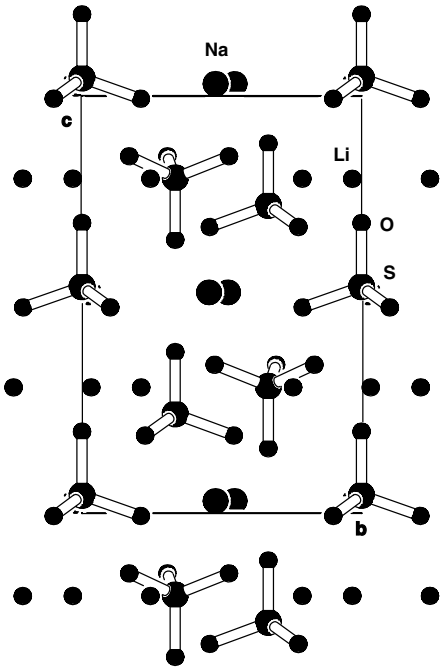

Figure 3. Projection of the unit-cell content of β-$LiNaSO_4$ down the a-axis.

centre gives a mirror plane perpendicular to $\boldsymbol{c}$ (the obtained twin law), we conclude that the enantiomorphic coordinates of Morosin correspond to the twin crystal observed in the present crystal structure determination. The results shown here then become the best determination of the crystal structure of $LiNaSO_4$. The problem of obtaining twinned crystals has already been observed in $LiKSO_4$, but in that case is possible to obtain untwinned crystals [31–33], although we have not been able to do this in $LiNaSO_4$.

The observation of the twinned crystal is in agreement with the results obtained by Junke *et al* [22] by NMR, where 12 rather than six different EFG tensors fall into two sets with six tensors each. The two sets transform into each other by a mirror plane perpendicular to the trigonal axis, which is the twin law obtained in the present crystal structure determination. The crystal structure of $LiNaSO_4$ at room temperature can be described as a framework of corner-shared LiO_4 and SO_4 tetrahedra with Na filling the cavities within the framework. The Na ion displays distorted bicapped trigonal prism coordination with respect to oxygen atoms, while this ion displays an octahedron in Na_2SO_4.

If the structures at room temperature of $LiKSO_4$ [31], $LiNH_4SO_4$ [34] and $LiNaSO_4$ are compared, all the unit-cell SO_4 tetrahedra are observed to have the same orientation in $LiKSO_4$; the relationship between up and down is 2:1 in $LiNaSO_4$ and 1:1 in $LiNH_4SO_4$. This explains the different spontaneous polarizations of the three compounds at room temperature. Spontaneous polarization is highest in $LiKSO_4$; it is poor in $LiNaSO_4$, where, moreover, the twin law reduces it, and it is low in $LiNH_4SO_4$, where the polarization axis is normal to the pseudo-trigonal axes and the polarization is more dipolar than charge polarization type [34].

Table 3 shows the observed frequencies in Raman scattering. The crystal structure of Li_2SO_4 [8] shows two lithium atoms, which are not equivalent by a symmetry operation, one with a range of O–Li–O angles 106.3°–115.7° and the second between 89.8° and 124.8°. This explains the shift of external mode t^{Li} (421.3(2) and 438.22(7) cm^{-1}), while the $LiNaSO_4$ only

Table 3. The observed frequencies (cm^{-1}) in Raman scattering of $LiNaSO_4$, Na_2SO_4 and Li_2SO_4. Values without e.s.d were not analytically fitted. The given value is the position of the peak maximum.

External modes			Internal modes		
$LiNaSO_4$	Na_2SO_4	Li_2SO_4	$LiNaSO_4$	Na_2SO_4	Li_2SO_4
55	54.8(4)	51.68(8)		446.9(4)	520.3(2)
80	75.44(6)	73.60(7)	475.29(9)	462.3(5)	609.75(4)
		86.91(11)	621.39(12)	617.3(2)	617.74(12)
		93			648.02(4)
103.1(7)	101		640.80(7)	628.9(4)	665.83(12)
114.7(7)		112.59(12)	656.6(2)	642.8(8)	
	131.45(8)	132.9(2)	970.05(8)		
		146.4(7)	991.15(17)		1005.14(2)
150.7(6)	155.47(14)	158	996.98(7)	990.12(2)	
	248.4(9)		1023.78(17)		
		352.5(5)	1066.8(3)		
		394.4(4)	1078.2(8)		
401.62(11)		421.3(2)	1099.3(6)	1098.9(3)	1120.54(4)
		438.22(7)	1121.09(16)	1129.2(3)	1145.0(2)
			1136.27(10)		1165.8(2)
			1150.9(3)	1150.00(19)	1184.9(2)
			1171.56(6)		1193.74(8)

Table 4. Bond lengths (Å) and angles (°) for $LiNaSO_4$. Symmetry transformations used to generate equivalent atoms: (i) $= -y+2, x-y+1, z$ (ii) $= y, x, z+1/2$ (iii)$x-y+1, -y+1, z+1/2$ (iv) $= -x+y+1, -x+1, z$ (v) $= -x+y+1, -x+2, z$ (vi) $= -y+1, x-y, z$ (vii) $= -y+1, x-y+1, z$ (viii) $= -x+y, -x+1, z$.

Na–O(6)(i)	2.394(2)	Na–O(3)	2.4069(14)
Na–O(4)(ii)	2.4156(14)	Na–O(5)(iii)	2.473(2)
Na–O(2)	2.4964(15)	Na–O(5)(iv)	2.679(2)
Na–O(4)(ii)	2.9593(14)	Na–O(6)(iv)	2.975(2)
S(1)–O(4)	1.4704(10)	S(1)–O(4)(v)	1.4704(10)
S(1)–O(4)(i)	1.4704(10)	S(1)–O(1)	1.504(2)
S(2)–O(2)	1.462(2)	S(2)–O(5)(vi)	1.4724(12)
S(2)–O(5)	1.4724(12)	S(2)–O(5)(iv)	1.4724(12)
S(3)–O(3)	1.463(2)	S(3)–O(6)(vii)	1.4632(13)
S(3)–O(6)	1.4632(13)	S(3)–O(6)(viii)	1.4632(13)
Li–O(4)(ii)	2.031(3)	Li–O(5)	1.922(3)
Li–O(6)(i)	1.891(3)	Li–O(1)	2.040(3)
O(4)–S(1)–O(4)(v)	109.56(5)	O(4)–S(1)–O(4)(i)	109.56(5)
O(4)(v)–S(1)–O(4)(i)	109.56(5)	O(4)–S(1)–O(1)	109.38(5)
O(4)(v)–S(1)–O(1)	109.38(5)	O(4)(i)–S(1)–O(1)	109.38(5)
O(2)–S(2)–O(5)(iv)	110.24(6)	O(2)–S(2)–O(5)	110.24(6)
O(5)(iv)–S(2)–O(5)	108.69(6)	O(2)–S(2)–O(5)(vi)	110.24(6)
O(5)(iv)–S(2)–O(5)(vi)	108.69(6)	O(5)-S(2)-O(5)(vi)	108.69(6)
O(3)–S(3)–O(6)(vii)	110.35(7)	O(3)–S(3)–O(6)	110.35(7)
O(6)(vii)–S(3)–O(6)	108.58(7)	O(3)–S(3)–O(6)(viii)	110.35(7)
O(6)(vii)–S(3)–O(6)(viii)	108.58(7)	O(6)–S(3)–O(6)(viii)	108.58(7)

shows a lithium atom in the asymmetric unit and one translational mode at 401.62(11) cm^{-1}. The role of oxygen atoms in the $LiNaSO_4$ structure is different (table 4), thus O(1) links with three Li ions, O(2) and O(3) with three Na atoms and the remaining oxygen atoms O(4),

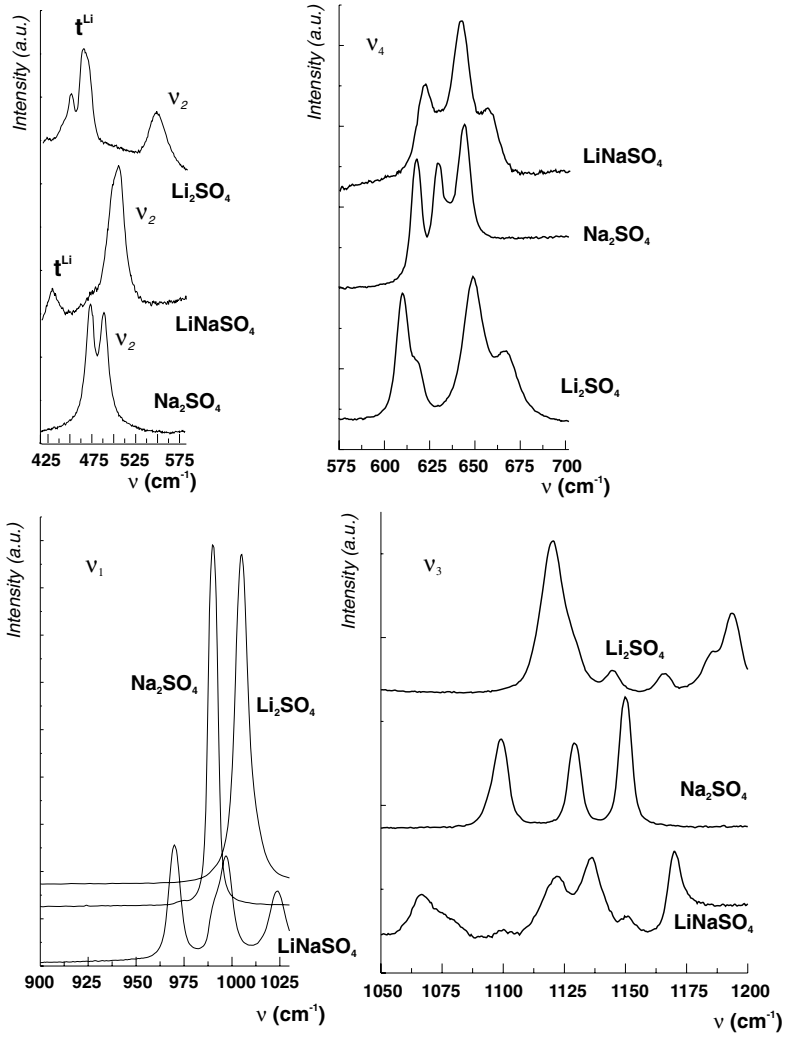

Figure 4. Different zones of Raman scattering of Li_2SO_4, Na_2SO_4 and $LiNaSO_4$.

O(5) and O(6) with two Na ions and one Li ion. This makes the S–O(1) bond length the longest (1.504(2) Å), while the S–O(2) and S–O(3) bonds are the shortest (average value 1.462(1) Å). This explains the three different internal $\nu_1(SO_4)$ modes in $LiNaSO_4$ Raman spectra (970.05(8), 996.98(7) and 1023.78(17) cm^{-1}), while the $\nu_1(SO_4)$ mode is at 990.12(2) in Na_2SO_4 and 1005.14(2) in Li_2SO_4. The splitting of the 996.98(7) mode in $LiNaSO_4$ to 991.15(17) and 996.98(7) (figure 4) is related to the two types of S–O(4), S–O(5) and S–O(6) length, the first close to 1.47 Å and the second close to 1.46 Å. The sulfate ion has a site symmetry C_3 in $LiNaSO_4$ and shows one $\nu_2(SO_4)$ mode at 475.29(9) cm^{-1}. This ion has a pseudo-C_3 symmetry in Li_2SO_4 and the $\nu_2(SO_4)$ mode appears at 520.3(2) cm^{-1} (the width of the peak in the second compound is larger than the first case). Finally the SO_4 ion has the site group D_2 symmetry in Na_2SO_4, so two $\nu_2(SO_4)$ modes at 446.9(4) and 462.3(5) cm^{-1} (figure 4).

The determination of the binary phase diagram Li_2SO_4–Na_2SO_4 is not easy. The different ATD analyses make it possible to deduce that the transition temperatures depend on the type

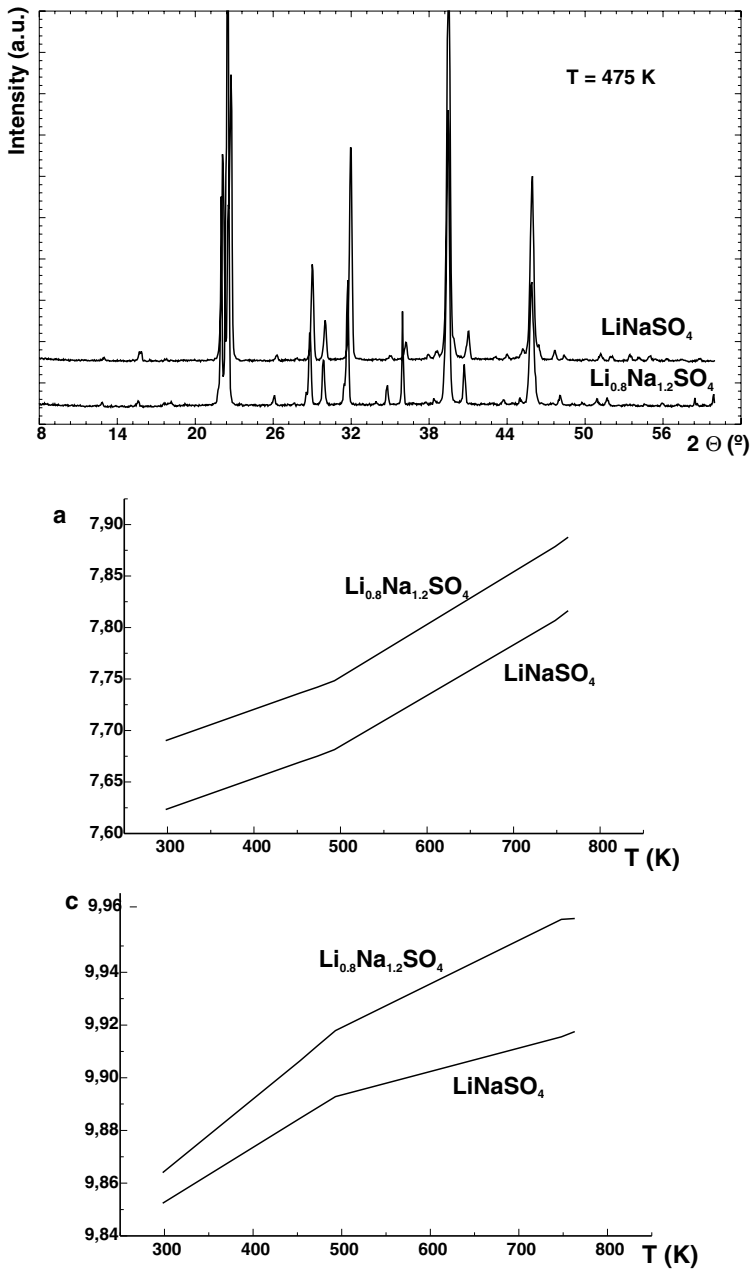

Figure 5. X-ray powder pattern of $LiNaSO_4$ and $Li_{0.8}Na_{1.2}SO_4$ at 475 K. Pt peaks at 39 and 45.5° are used as the standard reference. Bottom, variation of the cell parameters of $LiNaSO_4$ and $Li_{0.8}Na_{1.2}SO_4$ versus temperature.

of process (warming or cooling) and the cooling or warming rates. Moreover, it is not possible to analyse the high-temperature phases at room temperature, because they are not stable at this temperature when they are obtained by quenching.

From the x-ray powder analysis, we observe the formation of the mixed crystal $Li_{2-x}Na_xSO_4$ phase at low temperature in the compositional range $1 \leqslant x \leqslant 1.22$ (figure 5).

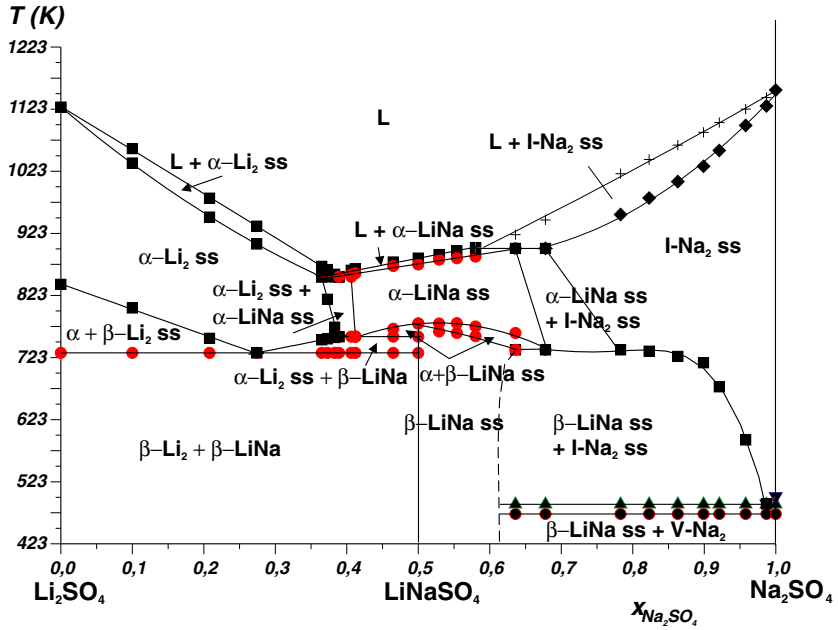

Figure 6. Phase diagram of the binary system Li_2SO_4– Na_2SO_4.
(This figure is in colour only in the electronic version)

The cell parameters increase in this compositional range; the influence of the temperature in the values of these parameters is shown in figure 5. The slope change in the variation of the cell parameters of the $Li_{2-x}Na_xSO_4$ at about 500 K suggests the possibility of phase transition at this temperature, but this has not been confirmed by x-ray diffraction. The phase diagram is shown in figure 6. The points of the diagram are from DTA data. The composition of each zone is from x-ray data. The curve of the diagram has been obtained by polynomial fitting of the different experimental points.

A eutectic reaction L $\leftrightarrow$ α-Li_2SO_4 (ss) + α-$LiNaSO_4$ (ss) takes place at 852.9 K. The composition at the eutectic point is a molar fraction of Na_2SO_4 equal to 0.389 mole. There are two eutectoid reactions: α-Li_2SO_4 (ss) $\leftrightarrow$ β-Li_2SO_4 + β-$LiNaSO_4$ at 730.6 K with molar fraction of the eutectoid point 0.274 and α-$LiNaSO_4$ (ss) $\leftrightarrow$ I-Na_2SO_4 (ss) + β-$LiNaSO_4$ (ss) at 735.5 K with composition 0.678. A peritectoid reaction L + I-Na_2SO_4 (ss) $\leftrightarrow$ α-$LiNaSO_4$ (ss) occurs at 900.2 K. We have observed that an increase of the cooling rate produces an enlargement of the I-Na_2SO_4 domain and a displacement of the α-$LiNaSO_4$ (ss) + I-Na_2SO_4 (ss) zone to richer compositions in lithium.

4. Conclusions

The structure of $LiNaSO_4$ has been correctly determined. This result and the crystal structures of Li_2SO_4 and Na_2SO_4 explain the NMR spectrum and the low spontaneous polarization of $LiNaSO_4$ as well as the Raman scattering of Li_2SO_4, $LiNaSO_4$ and Na_2SO_4. A new phase diagram of the binary system Li_2SO_4–Na_2SO_4 is deduced using a lower cooling rate. From this diagram the mixed crystals of $Li_{2-x}Na_xSO_4$ with $1 \leqslant x \leqslant 1.22$ are observed for the first time.

References

[1] Nacken R 1907 *Neues Jahrb. Mineral. Geol. Beilageband* **24** 42
[2] Schroeder K and Kvist A 1968 *Z. Naturf.* **23** 773
[3] Schroeder K, Kvist A and Ljungmark H 1972 *Z. Naturf.* **27** 1252
[4] Suleiman B M, Gustavsson M, Karawacki E and Lundén A 1997 *J. Phys. D: Appl. Phys.* **30** 2553
[5] Nilsson L, Thomas J O and Tofield B C 1980 *J. Phys. C: Solid State Phys.* **13** 6441
[6] Karlsson L and McGreevy R L 1995 *Solid State Ion.* **76** 301
[7] Forland T and Krogh-Moe J 1957 *Acta Chem. Scand.* **11** 565
[8] Alcock N W, Evans D A and Jenkins H D B 1973 *Acta Crystallogr.* B **29** 360
[9] Mellander B E and Lazarus D 1985 *Phys. Rev.* B **31** 6801
[10] Tärneberg R and Lundén A 1996 *Solid State Ion.* **90** 209
[11] Kracek F C 1929 *J. Phys. Chem.* **33** 1281
[12] Eysel W 1973 *Am. Mineral.* **58** 736
[13] Murray R M and Secco E A 1978 *Can. J. Chem.* **56** 2616
[14] Davies J E D and Sandford E F 1975 *J. Chem. Soc. Dalton Trans.* **19** 1912
[15] Cody C A, Dicario L and Darlington R K 1981 *J. Inorg. Nucl. Chem.* **43** 398
[16] Naruse H, Tanaka K, Morikawa H, Marumo F and Mehrotra B N 1987 *Acta Crystallogr.* B **43** 143
[17] Rasmussen S E, Jorgensen J E and Lundtoft B 1996 *J. Appl. Crystallogr.* **29** 42
[18] Eysel W, Höfer H H, Keester K L and Hahn Th 1985 *Acta Crystallogr.* B **41** 5
[19] Nord A G 1973 *Acta Chem. Scand.* **27** 814
[20] Mellander B E, Granéli B and Roos J 1990 *Solid State Ion.* **40–1** 162
[21] Morosin B and Smith D L 1967 *Acta Crystallogr.* **22** 906
[22] Junke K D, Mali M, Roos J and Brinkmann D 1988 *Solid State Ion.* **28/30** 1329
[23] Teeters D and Frech R 1982 *Phys. Rev.* B **26** 4132
[24] Teeters D and Frech R 1982 *J. Chem. Phys.* **76** 799
[25] Dharmasena G and Frech R 1995 *J. Chem. Phys.* **102** 6941
[26] Sakuntala T and Arora A K 2000 *J. Phys. Chem. Solids* **61** 103
[27] Sheldrick G M 1997 *SHELXS A Computer Program for Crystal Structure Determination* Univ. Göttingen
[28] Sheldrick G M 1993 *SHELXL A Computer Program for Crystal Structure Determination* Univ. Göttingen
[29] Flack H D 1983 *Acta Crystallogr.* A **39** 867
[30] Rodríguez-Carvajal J 1996 *FULLPROF* version 3.1c, Laboratoire Leon Brillouin, Paris
[31] Solans X, Calvet M T, Martínez-Sarrión M L, Mestres L, Bakkali A, Bocanegra E, Mata J and Herraiz M 1999 *J. Solid State Chem.* **148** 316
[32] Ortega J, Extxebarría J and Breczewski T 1993 *J. Appl Crystallogr.* **26** 549
[33] Solans X, Calvet M T, Martínez-Sarrión M L, Mestres L, Bakkali A, Bocanegra E, Mata J and Herraiz M 2001 *J. Solid State Chem.* **156** 251
[34] Solans X, Mata J, Calvet M T and Font-Bardia M 1999 *J. Phys.: Condens. Matter* **11** 8995